



Analysis and design of the Alfvén wave antenna system for the SUNIST spherical tokamak

Yi Tan*, Zhe Gao, Yexi He

Department of Engineering Physics, Tsinghua University, Beijing 100084, China

ARTICLE INFO

Article history:

Received 26 May 2008

Received in revised form

13 November 2008

Accepted 9 December 2008

Available online 20 January 2009

Keywords:

Alfvén wave current drive

Antenna system

SUNIST spherical tokamak

ABSTRACT

Analysis and design of the Alfvén wave antenna system for the SUNIST spherical tokamak are presented. Two candidate antenna concepts, folded and unfolded, are analyzed and compared with each other. In the frequency range of Alfvén resonance the impedance spectrums of both two concept antennas for major modes are numerically calculated in a 1-D MHD framework. The folded concept is chosen for engineering design. The antenna system is designed to be simple and requires least modification to the vacuum vessel. The definition of the antenna shape is guided by the analyses with constraints of existing hardware layouts. Each antenna unit consists of two stainless steel straps with a thickness of 1 mm. A number of boron nitride tiles are assembled together as the side limiters for plasma shielding. Estimation shows that the structure is robust enough to withstand the electromagnetic force and the heat load for typical discharge duty cycles.

© 2008 Elsevier B.V. All rights reserved.

1. Introduction and motivation

Spherical tokamak (ST) [1] has shown its attractiveness of high beta (the ratio of plasma pressure to magnetic field pressure) and good stability properties from a number of ST experiments [2–4]. However, the difficulties of startup and/or current drive in ST, which are caused by its slim central stack, are the obstacles that have to be leaped over before its application of fusion plant or component test facility (CTF). Many non-inductive startup and/or current drive methods therefore have been applied to STs. Nevertheless, some promising current drive methods in conventional tokamaks, such as electron cyclotron wave (ECW) and lower hybrid wave (LHW), have encountered difficulties in applying to ST plasmas, which have very high dielectric constants.

Alfvén waves was considered as an attractive mechanism of driving plasma current because of its potential high efficiency, no density limit and the convenience of high power RF generating [5]. The difficulties brought by high dielectric constants of ST plasmas are absent for Alfvén waves. Indeed, the experimental evidences of Alfvén wave current drive (AWCD) have been observed in the Phaedrus-T [6] and the TCABR [7] tokamaks without seeing serious trapped electron effects that was previously thought to reduce or eliminate the effects of current drive [8]. Of course, these two are both conventional tokamaks with relatively higher aspect ratio $A = R_0/a > 3$, where R_0 and a are the major radius and minor radius

respectively, and, moreover, both experiments were working in the plateau regime. In banana regime, the case of ST, how the larger fraction of trapped electrons deteriorates the driving efficiency is still uncertain. Ponderomotive force applied on non-resonant electrons provided by helicity injection was proposed to be able to overcome the trapped electron effects [9]. However, this non-resonant drive force was theoretically proved to be cancelled out when nonlinear stress forces were taken into account [10,11]. Although localized current drive close to axis [12] can decrease the influence of trapped electrons and neoclassical effects such as Ware pinch effects [5] and bootstrap-like mechanism [13] has the potential of recovering the momentum absorbed by trapped electrons in quasi-steady status, all these schemes need to be experimentally verified.

Beyond the scientific attraction in clarifying the scheme of Alfvén wave current drive, the low cost of low frequency (<10 MHz) generators, as well as the possibility of high driving efficiency, still show great attraction for AWCD experiments in a ST. Moreover, at least, the heating effect of Alfvén wave is reserved without much adjustment required. Even more, it is found that the AW power absorbed by trapped electrons would be rather beneficial for inducing poloidal and toroidal rotations to suppress transport [14].

A preliminary plan of AWCD on the ETE spherical tokamak [15], in fact, has been proposed, but seems not to be actualized finally. However, its idea and design are very helpful for our AWCD program on the SUNIST spherical tokamak. SUNIST is located at Tsinghua University, Beijing, China and has been started discharges since the end of 2002 [16]. Its main parameters are shown in Table 1. This paper intends to describe the analyses and the engineering design of the Alfvén wave antenna for its AWCD program.

* Corresponding author. Tel.: +86 10 62776446; fax: +86 10 62782658.
E-mail address: tanyi@sunist.org, tanyi@tsinghua.org.cn (Y. Tan).

Table 1
The main parameters of SUNIST.

Parameter	Symbol	Value
Major radius	R_0	30 cm
Minor radius	a	23 cm
Elongation ratio	κ	1.6
On-axis magnetic field	B_0	1500 G
Peak electron density	n_0	$\sim 3 \times 10^{13} \text{ cm}^{-3}$
Typical plasma current	I_p	$\sim 30 \text{ kA}$
Working gas		H_2
Pulse length		$< 30 \text{ ms}$

Cuperman et al. have completed a series of numerical research [17–19] on Alfvén wave characters in ST plasmas, including the effects of toroidicity coupling, plasma elliptic cross-section coupling and triangularity coupling. The following results are shown from their research. (a) The frequency range of Alfvén continuum increases with a factor of 2.5 when the aspect ratio decreases from 10 to 1.1, while the magnitude of the power absorption remains in the same order of magnitude [17]. (b) The wave power launched from an antenna located at the outer region of vacuum vessel is most efficiently coupled in outer regions of plasmas [18]. (c) The power deposition in TAEs (toroidal Alfvén eigenmodes), EAEs (elliptic Alfvén eigenmodes) and NAEs (non-circular Alfvén eigenmodes) is significantly larger than those predicted for the Alfvén continuum eigenmodes in a circular cross-section plasma and may be achieved by selecting proper phase and frequency for antennas [18].

Although many interesting characters of Alfvén wave are induced in ST plasmas by the low aspect ratio and the strongly shaped plasma cross-section, these results give us the confidence of utilizing a circular cross-section cylindrical model for our analyses. The main purposes of the analyses are to estimate the loading impedance of the plasmas and to determine a frequency range for the output of the RF generator. If the impedances varying in the same order of magnitude are tolerable for our RF generator, the simple and fast cylindrical model is adequate to realize these objectives according to result (a). 2-D analysis without any geometrical limitations, which is precise but quite complex and consumes a huge amount of computer resources, is not essential for designing an antenna system which has significant tolerance. Discovery of Alfvén eigenmodes induced by cross-section symmetry breaking of course would be the main experimental interests. However, our attention should be mainly focused on the impedance of Alfvén continuum in the step of designing the antenna system. The attempts of utilizing those Alfvén eigenmodes should be our efforts after we have obtained sufficient experimental understanding of them. Additionally, the coupling impedance is affected by impurities. For these complicated reasons, the actual impedance therefore can be experimentally measured only. The analysis here merely gives an estimation of the impedances.

Result (b) is also favorable for us to use cylindrical model. Since the toroidal field in the plasma column of SUNIST differs in a factor of 7 from inboard side to outboard side, the Alfvén resonant frequency and other characters of Alfvén waves are hard to be considered in 1-D cylindrical model. However, if the wave energy is mostly deposited in the outer region of the plasma column, it is more confident for us to treat the cylindrical model as a small circular outer region in the strongly shaped ST plasma column. For example, in the outer region, the relative toroidal field in the SUNIST device only varies from 0.6 (outer boundary) to 1 (center of the plasma column).

The paper is organized as follows. In Section 2 the frequency range of Alfvén resonance in SUNIST is estimated. Two concept designs of the antenna are described in Section 3. Next, in Section 4, the modeling and analyses of the two concept antennas are pre-

sented. The engineering design of the antenna is shown in Section 5. Finally, Section 6 gives a short summary.

2. The frequency range of Alfvén resonance

The energy is transferred from RF waves to plasmas through the dissipation of kinetic Alfvén waves (KAW), when the frequency of the RF wave matches the local Alfvén wave frequency, $\omega_A(r) = k_{\parallel}(r)B(r)/\sqrt{\mu_0 m_i n_i(r)}$. Here m_i and $n_i(r)$ are ion mass and density respectively. $k_{\parallel}(r) = N/R\{1 + M/[Nq(r)]\}$ is the wave number parallel to the local magnetic field. N and M are toroidal and poloidal mode numbers respectively. The profile of safety factor q is selected to be corresponding to a peak current density profile. The density profile is set to be parabolic. In the ohmic plasmas of SUNIST, the dependence of radial resonant position on frequency in different modes is shown in Fig. 1. It is obvious that resonant positions move to periphery when frequency is high. The local Alfvén wave frequency in the inner region also rises because the toroidal field significantly increases. In order to effectively deposit wave energy and to avoid unexpected density rise [20], the conversion of KAW should be located at the interior of plasma column rather than the periphery. The output frequency of the RF generator hence must be constrained in a certain range. In practice, we choose 1.0 MHz as the maximum output frequency for our RF generator. This frequency would still be enough even if the Alfvén continuum is expanded in actual ST plasmas. Since the impedances of $|N| = 2$ modes are quite small at frequency less than 0.4 MHz (can be seen in Section 4.2), radial profiles of $|N| = 2$ modes are started from 0.4 MHz in Fig. 1(b).

3. Concept design of the antenna system

The main task of the antenna in AWCD experiments is to excite a perturbation of magnetic field \tilde{B} parallel to the equilibrium magnetic field $\tilde{B}_0 = \tilde{B}_{0z} + \tilde{B}_{0\theta}$, where \tilde{B}_{0z} and $\tilde{B}_{0\theta}$ are the toroidal and poloidal equilibrium magnetic field respectively, with required spatial structures (called modes) in the plasma column. It is typically achieved by assembling poloidal current carrying loops surrounding the plasma column. However, loops with fully extension in poloidal direction cannot be implemented in STs because of the very tight configuration of central region.

Two compromising antenna concepts, folded and unfolded, in the geometry of SUNIST device are shown in Fig. 2. They both consist of straps with about 90° extension in poloidal direction. Two straps (including return limb in folded concept) in the same toroidal position are defined as a module. In general, more modules installed, more flexibly the wave field structure is controlled by phasing the current in straps. Nevertheless, for such a small volume of the vacuum vessel and limited number of windows in the SUNIST device, it is quite difficult to install more than four modules. The excellences of these two concepts are obvious. The folded one is easy to connect with RF generator (since all the four terminals of one module are collected together in one window) and occupies fewer windows. Nevertheless, the unfolded one is quite simple and much easier to be manufactured and installed.

Another important issue of ST plasmas is the pitch angle of the magnetic field line at the outer region. The electrical field parallel to the field line may cause certain power loss and impurity production. In typical ohmic discharges of SUNIST ($I_p = 30 \text{ kA}$, $B_{0z} = 1500 \text{ G}$), the pitch angle is about 16.5° . It is therefore better to make the antenna module slightly rotatable. The folded concept is obviously easier to be adjusted.

4. Analysis of the antenna system

The antenna system is analyzed as follow. First, in Section 4.1, a 1-D MHD model is introduced. In this model, the dependence

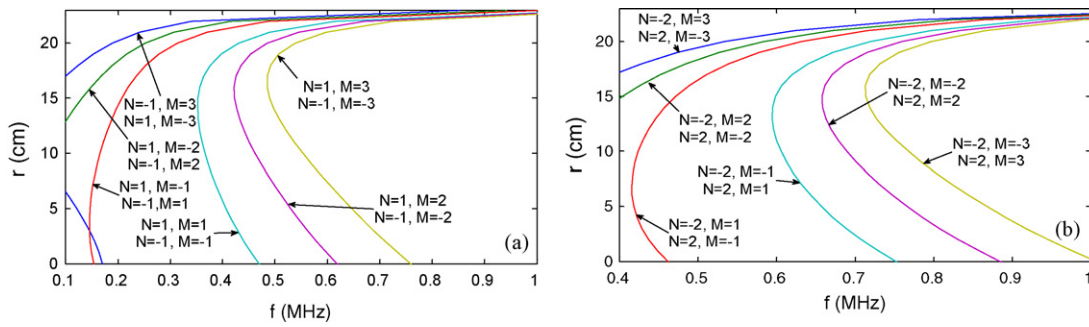


Fig. 1. The dependence of radial resonant position on frequency for the main modes (a) $|N|=1$ modes and (b) $|N|=2$ modes.

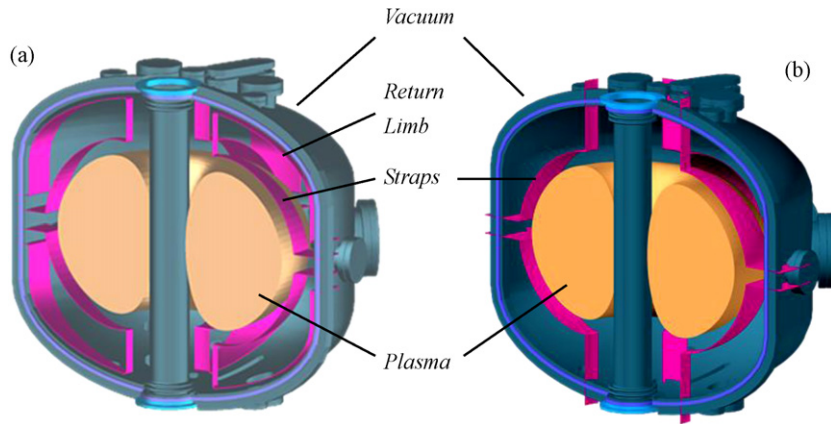


Fig. 2. Two concept designs of the antenna for the SUNIST spherical tokamak (a) folded and (b) unfolded.

of impedance on frequency for each single ideal mode are presented and discussed in Section 4.2. The coefficients of each ideal mode are calculated by decomposing the current density distribution of the antenna system into a sum of spatial harmonics in Section 4.3. Finally, in Section 4.4, the impedance spectrums of the actual antenna system at several working points are obtained by summing up the weighted impedances of all significant modes.

4.1. The 1-D MHD model

As described in Section 1, if we only want to estimate the impedance spectrum and give preliminary power deposition pictures in plasmas, it is still valid to treat the strongly shaped plasma–antenna–wall system as cylindrical. Therefore, a simple model in the cylindrical geometry shown in Fig. 3 is utilized in the analyses. This model consists of a plasma column (region I, $r < r_p$), two sheaths carrying currents with spatial modes in opposite directions (folded configuration) or one current carrying sheath (unfolded configuration) and an outer cylindrical wall made by per-

fect conductor. Region II is the region between the antenna and plasma column ($r_p < r < r_a$). In the folded configuration, region III and IV are defined by the region between the antenna and the return limb ($r_a < r < r_b$) and by the region between the return limb and wall ($r_b < r < r_w$) respectively. In the unfolded configuration, region III is not defined but region IV is defined by the region between the antenna and the wall ($r_a < r < r_w$).

The process of solving the wave fields in 1-D MHD model has been well described in [21,22]. But for the sake of integrality of this paper, it is briefly outlined below. Especially, the boundary condition at return limb is introduced and a correction is made on the description in [22].

We set all the time and space dependence of the perturbation quantities to be $\exp\{i[M\theta + Nz/R - (\omega + i\nu)t]\}$, where $\nu \rightarrow 0^+$ is a small artificial added dissipation to make calculation easy when singularity encountered [21] but has nothing to do with the results.

In region I, the solution of the wave equations can be written as

$$B_{||}^I(r, \theta, z, t) = \sum_{N=-\infty}^{\infty} \sum_{M=-\infty}^{\infty} B_{NM}^I(r) e^{i[M\theta + Nz/R - (\omega + i\nu)t]} \quad (1)$$

and

$$E_{\perp}^I(r, \theta, z, t) = \sum_{N=-\infty}^{\infty} \sum_{M=-\infty}^{\infty} E_{NM}^I(r) e^{i[M\theta + Nz/R - (\omega + i\nu)t]}, \quad (2)$$

where $B_{||}^I$ is the component of the wave magnetic field parallel to the equilibrium magnetic field and E_{\perp}^I is the perpendicular component of the wave electric field. The radial profile of these two field

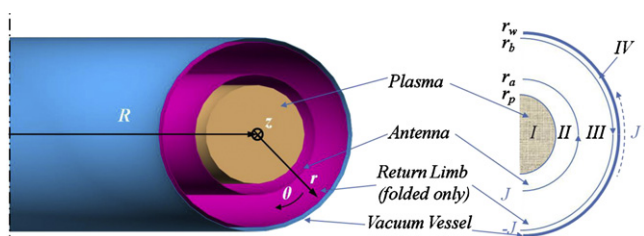


Fig. 3. The cylindrical geometry and the corresponding model for 1-D MHD analysis (r_p , r_a , r_b and r_w are the radial positions of the plasma edge, antenna, return limb and the wall of vacuum vessel. The return limb, r_b and region III are presented in folded configuration only).

components are coupled with each other,

$$\begin{cases} A \frac{1}{r} \frac{d}{dr} [rE_{NM}^I(r)] = k_{\perp} G E_{NM}^I(r) + (A - k_{\perp}^2) B_{NM}^I(r) \\ A \frac{d}{dr} B_{NM}^I(r) = \frac{c}{i\omega} (G^2 - A^2) E_{NM}^I(r) - k_{\perp} G B_{NM}^I(r) \end{cases} \quad (3)$$

where

$$A = \left(\frac{\omega}{C_A}\right)^2 \frac{1}{1 - (\omega/\omega_{ci})^2} - k_{\parallel}^2 \quad (4)$$

$$G = \left(\frac{\omega}{C_A}\right)^2 \frac{\omega/\omega_{ci}}{1 - (\omega/\omega_{ci})^2} - \frac{2}{r} \frac{B_{0\theta}}{B_{0z}} k_{\parallel} \quad (5)$$

and

$$k_{\perp} = \frac{M}{r} - \frac{N}{R} \frac{B_{0\theta}}{B_0} \quad (6)$$

$$k_{\parallel} = \frac{M}{r} \frac{B_{0\theta}}{B_0} + \frac{N}{R}. \quad (7)$$

In the three (folded model) or two (unfolded model) vacuum regions, region II, III (folded model) and IV, only the magnetic field perturbation in z direction is concerned. Since the wave number of low frequency EM wave in vacuum, $k_{vac} = \omega/c \approx 0.01 \text{ m}^{-1}$, is far less than the absolute value of toroidal wave numbers, $|k_z| = |N/R| > 3 \text{ m}^{-1}$, ($N \neq 0$), the radial functions of magnetic field perturbation in these regions are similar to typical vacuum magnetostatic field in cylindrical geometry, which are composed by series of modified Bessel functions,

$$B_z^j(r, \theta, z, t) = \sum_{N=-\infty}^{\infty} \sum_{M=-\infty}^{\infty} \left[A_{NM}^j I_M \left(\frac{N}{R} r\right) + B_{NM}^j K_M \left(\frac{N}{R} r\right) \right] e^{i[M\theta + Nz/R - (\omega + iv)t]} \quad (j = \text{II, III, IV}). \quad (8)$$

Besides Eqs. (3) and (8), the wave fields must satisfy the following boundary conditions. At $r = r_p$, the plasma–vacuum boundary, fields must be continued,

$$B_{\parallel}^I|_{r_p-} = \frac{k_{\parallel}}{k_z} B_z^I|_{r_p+} \quad (9)$$

and

$$E_{\perp}^I|_{r_p-} = \frac{i\omega}{ck_z k_{\parallel}} \frac{dB_z^I}{dr} |_{r_p+}. \quad (10)$$

It should be noted that $k = \sqrt{k_{\parallel}^2 + k_{\perp}^2}$ replaced k_z in [22]. This should be incorrect.

At $r = r_a$, the layer of antenna strap, there is a field jump,

$$B_z^{\text{II}}|_{r_a-} - B_z^{\text{III}}|_{r_a+} = \frac{4\pi}{c} j_{\theta}, \quad (11)$$

$$\frac{dB_z^{\text{II}}}{dr} |_{r_a-} = \frac{dB_z^{\text{III}}}{dr} |_{r_a+}. \quad (12)$$

In the folded antenna model, at $r = r_b$, the return limb layer, there is another current jump like at $r = r_a$, except the direction of current.

$$B_z^{\text{III}}|_{r_b-} - B_z^{\text{IV}}|_{r_b+} = -\frac{4\pi}{c} j_{\theta}, \quad (13)$$

$$\frac{dB_z^{\text{III}}}{dr} |_{r_b-} = \frac{dB_z^{\text{IV}}}{dr} |_{r_b+}. \quad (14)$$

Finally, at $r = r_w$, the wall of vacuum vessel is treated as a perfect conducting boundary,

$$\frac{dB_z^{\text{IV}}}{dr} |_{r_w} = 0. \quad (15)$$

The process of solving Eqs. (3) and (8)–(15) is rather a reversed problem than an excitation problem. We first obtain a radial profile

of the perturbations in plasma column (region I) by numerical integration of Eq. (3), and then calculate the current in the antenna sheath needed to match such a perturbation through boundary conditions. After integrating the Poynting vector through the cylindrical surface at $r = r_p$ (or $r = r_a$, since there is no power deposition in vacuum) and the total current flow in the antenna, the impedance of antenna can be calculated by $Z_{NM} = 2P_{NM}/I^2$. This non-straightforward process is based on that the response of plasmas is linear. The initial conditions for the numerical integration of Eq. (3) are discussed in [23]: as $r \rightarrow 0^+$,

$$rE_{\perp}^I = r^m \hat{E}, \quad (16)$$

$$B_{\parallel}^I = r^m \hat{B}, \quad (17)$$

$$[G|_{r=0} - \text{sgn}(m)A|_{r=0}]\hat{E}|_{r=0} = i\omega\hat{B}|_{r=0}. \quad (18)$$

4.2. The results of ideal modes analyses

A number of modes have been analyzed. The dependences of impedance on frequency for several modes in unfolded model are shown in Fig. 4. In the frequency range 0–1 MHz, the impedances of $|N| > 2$ or $|M| > 3$ modes are much smaller than those of the modes of $|N| \leq 2$ and $|M| \leq 3$. That is why Fig. 4 shows only part of the analyzed modes (the traces of $|M| = 3$ modes are also hidden for clarity). Additionally, as can be seen from Fig. 4(b), the impedances are quite small for $|N| = 2$ modes if the frequency is less than 0.4 MHz. Thus, it is appropriate to start Fig. 1(b) from that frequency.

Fig. 5 demonstrates the effect of the radial positions of the return limb and wall on the antenna’s impedance. It is obvious that the coupling between antenna and plasmas is weakened when the return limb approaches the antenna strap. In our folded model, this effect is linear to all modes. For example, in the configuration of $r_b = 1.15r_p$, the impedances of folded antenna for all modes decrease to about 27% of unfolded antenna’s. That means we should bear an impedance loss of $\sim 70\%$ if the folded model is chosen for manufacture.

4.3. The harmonic analysis of the concept antennas

For harmonic analysis, the eight straps of concept antennas are modeled in a plane geometry (see Fig. 6), where axis y is mapped to the poloidal direction $\hat{\theta}$ in cylindrical geometry (Fig. 3). In this plane model, we have omitted the radial currents of feeders, and thus the folded concept is treated as two unfolded ones with opposite currents.

The actual current density distribution can be written as:

$$\vec{j} = J_0 e^{-i\omega t} f(y, z) \hat{y}, \quad (19)$$

where

$$f(y, z) = \begin{cases} e^{i\phi_k} & |y - y_k| < W, |y - y_k| < L \\ 0 & \text{else} \end{cases} \quad (k = 1, 2, \dots, 8). \quad (20)$$

W and L are the 1/2 width and 1/2 length of the straps respectively. ϕ_k is the initial phases of the currents in each straps. The current distribution can be represented by a series of harmonics:

$$\vec{j} = \sum_{N=-\infty}^{\infty} \sum_{M=-\infty}^{\infty} J_{MN} e^{i\left(\frac{M}{R}y + \frac{N}{R}z - \omega t\right)} \hat{y}. \quad (21)$$

Here, each harmonics has its helical form with the poloidal and toroidal mode numbers, M and N , and is expected to excite the field perturbations with the same helicity.

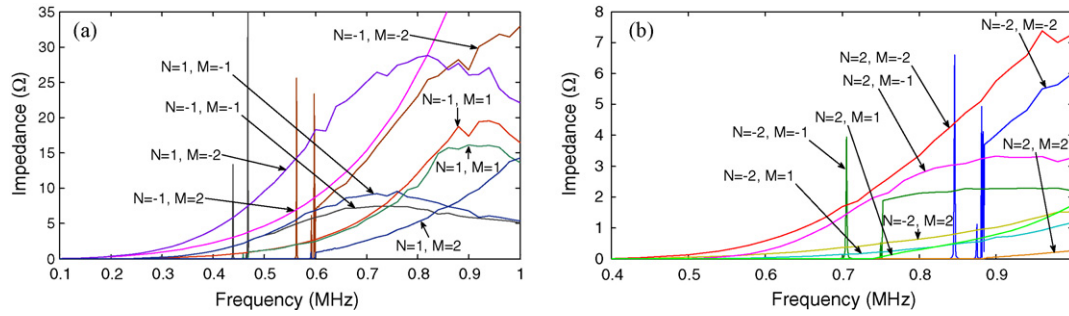


Fig. 4. The dependence of impedance on frequency for varies modes (a) $|N|=1, |M| \leq 2$ and (b) $|N|=2, |M| \leq 2$. Calculation settings: unfolded model, $r_p = 23$ cm, $r_a = 1.1r_p$, $r_w = 1.2r_p$.

The coefficients of each harmonics in Eq. (21) are obtained by the integration,

$$J_{MN} = \frac{J_0}{(2\pi)^2 r_a R} \int_0^{2\pi r_a} dy \int_0^{2\pi R} f(y, z) e^{-i((M/r_a)y + (N/R)z)} dz$$

$$= \frac{J_0}{\pi^2 r_a R} \frac{\sin\left(\frac{M}{r_a} L\right)}{\frac{M}{r_a}} \frac{\sin\left(\frac{N}{R} W\right)}{\frac{N}{R}} \sum_{k=1}^8 e^{i\left(\phi_k - \frac{M}{r_a} y_k - \frac{N}{R} z_k\right)} \quad (22)$$

Excitation of travelling wave might be favorable for current drive. Whether the harmonics excited are standing (the harmonics with the same absolute value of mode number are equally excited) or travelling (the harmonics with the same absolute value of mode number can be excited respectively) is determined by the phasing of straps. In our application, the RF generator can deliver two possible phase shift, $\pi/2$ or π , to nearby straps in either toroidal or poloidal direction. Thus, in toroidal direction, since the distance between two nearby straps is fixed to $\pi R/2$, a phase shift of $\pi/2$ or $-\pi/2$ between two nearby straps would excite a pure travelling wave. However, in poloidal direction, since the distance between two nearby straps is less than $3\pi r_a/2$ but greater than πr_a , a partial standing wave would be excited by $\pi/2$ or $-\pi/2$ phasing. Additionally, $\pm\pi$ phasing would excite pure standing wave in any cases.

4.4. The impedance spectrums of the antenna system at several working points

From Fig. 4, we can find a rough trend, i.e., higher frequency results in higher impedance. It seems that we should choose relatively higher working frequency for better coupling. Nevertheless, higher frequency would also leads to energy deposition closer to the plasma edge (as discussed in Section 2) and more modes excited.

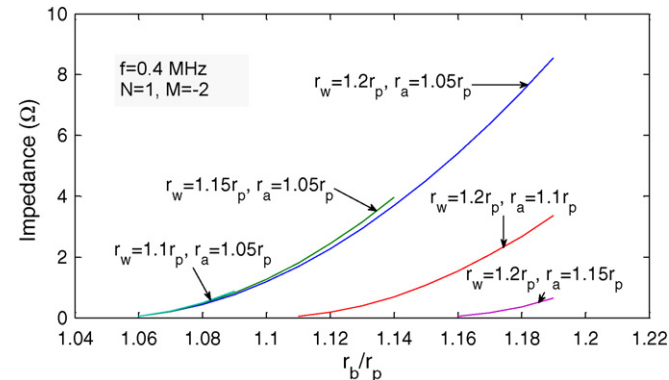


Fig. 5. The dependence of impedance on the radial position of the return limb and the wall in folded antenna concept.

The selection of working frequency therefore should be a compromise among impedance, the location of energy deposition and the number of excited modes. Besides the working frequency, phase shifts between two nearby feeding currents in toroidal ($\Delta\phi_t$) and poloidal ($\Delta\phi_p$) directions, which control the weights of current harmonics, are the other two key parameters of a working point. Comparing impedance spectrums is a direct method in determining a working point.

The impedance spectrums of the antenna system at certain working points can be obtained by summing up the impedance of each mode with the weight of corresponding current harmonics. In principal, a good working point should have a predominated mode and few stray modes. By manually comparing impedance spectrums at several frequencies and phase shifts for $N=1$ and $N=2$ modes, two optimistic working points for these two modes are selected out and are shown in Fig. 7(a) and (b) respectively.

For the working point (a), $f=0.4$ MHz, $\Delta\phi_t = 90^\circ$ and $\Delta\phi_p = -90^\circ$, the wave field excited is pure travelling in toroidal direction and poloidally partial standing. In addition, the impedances of the $N=1$ and $M>0$ modes are quite small at this frequency. These two properties result in a spectrum predominated by $N=1, M=-3$ or $M=-2$ modes at this working point. In contrast, a rather wide impedance spectrum is excited at the working point (b), $f=0.6$ MHz, $\Delta\phi_t = \pm 180^\circ$ and $\Delta\phi_p = -90^\circ$. Besides the wide spectrum, the impedances at the latter working point are also significantly smaller than the former. However, it is almost the best working point for $|N|=2$ modes excitation.

5. Engineering design of the antenna system

As discussed in Section 4.2, the impedance, in other words, the coupling efficiency of unfolded antennas is about three times as much as that of folded antennas. However, we still decide to select

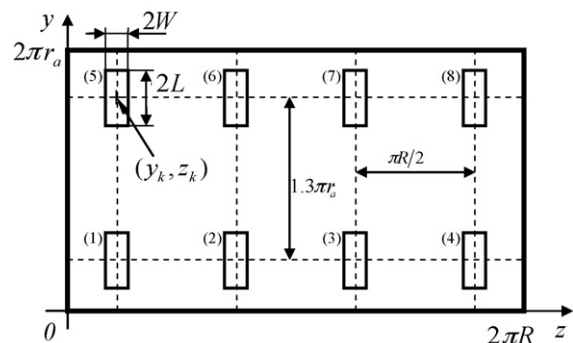


Fig. 6. Schematic of the eight antenna straps in plane geometry. Eight numbered rectangular boxes representing the antenna straps.

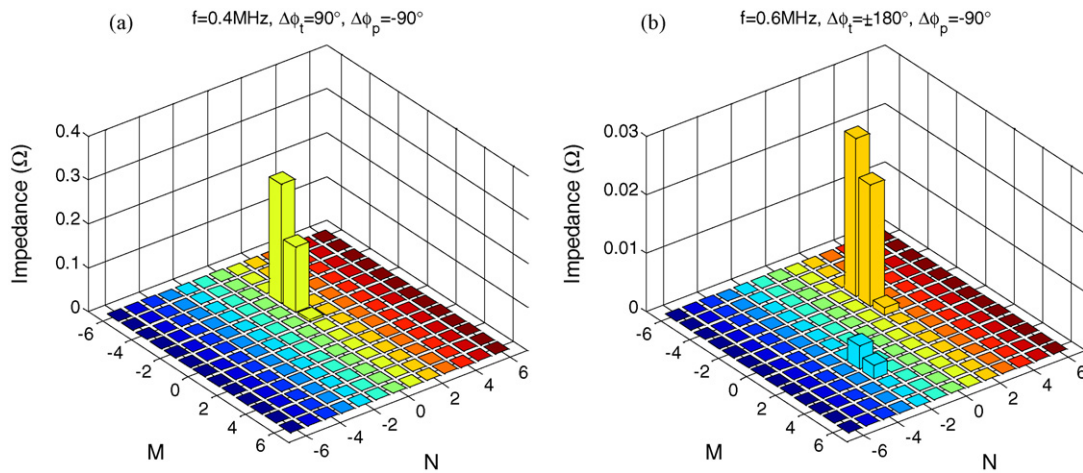


Fig. 7. The impedance spectra of unfolded antenna at two optimistic working points for $N=1$ modes (a) and $N=2$ modes (b).

the folded one as our antenna for manufacture because of the convenience in connecting to RF generator and less occupancies of windows (only four windows are occupied). The latter is even more important. The unfolded concept occupies as many as 12 windows, including several important windows used by basic diagnostics. This is intolerable for such a small tokamak device like SUNIST.

5.1. The structure of the antenna

The engineering design of the antenna system follows the guideline, i.e., the return limb should be positioned as close as possible to the wall of vacuum vessel for improving coupling efficiency. Hence, the shape of the return limb and the antenna strap are simply defined by offsetting the shape of vacuum vessel and the last closed flux surface of plasma column respectively. These shapes would have the most efficient utilization of limited space. The width of the antenna strap is limited by the diameter of windows and the poloidal extension angle is reduced in order not to envelop the other diagnostic windows.

Fig. 8 shows the cross-section 1/2 of one antenna module for manufacture in the geometry of SUNIST device. Fig. 9 is the 3-D view of one antenna module. In this design, the antenna strap and the return limb are made of 1 mm thick stainless steel with different width, which are 150 mm and 50 mm respectively. The cross-section is sufficient for conducting a short pulse (<30 ms) of <1 kA RF current. The resistive loss per pulse is only about 300J

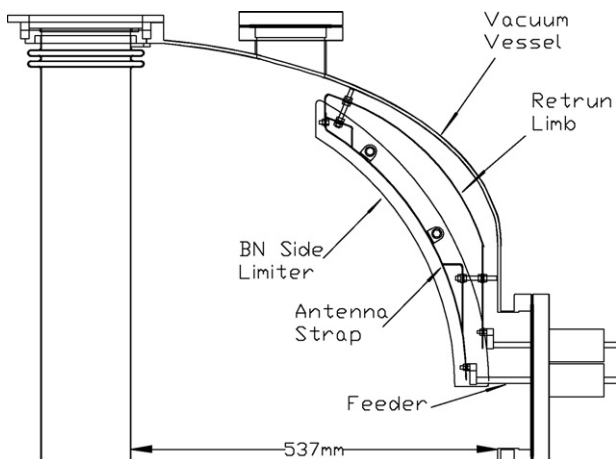


Fig. 8. Drawing of the engineering design of the antenna system.

and then the temperature rise due to the heat deposition can be neglected.

Four ceramic (Al_2O_3) washer insulated bolts fix the antenna module onto the vacuum vessel. These ceramic washers have a standoff voltage of 20 kV in the atmosphere and provide us a very simple solution for mounting the antenna structures. However, the main uncertainty of using these washers is to what extent the standoff voltage will be changed in our short pulse discharges. The standoff capabilities have to be continuously monitored in our experiments.

To simplify the manufacture, we choose side limiters consist of boron nitride (BN) plates rather than complicated Faraday shields as the plasma shielding components. Side limiters made of BN plates have been proven to have the ability of reducing edge power deposition [24]. This result gives us the opportunity of dramatically lowering the difficulties of the antenna system. In our antenna modules, a number of 50 mm × 50 mm × 6 mm and 25 mm × 50 mm × 6 mm BN plates are fixed on two stainless steel ribs by ceramic bolts and nuts, which prevent direct electrical contacts. The two ribs thus can be mounted directly on the antenna straps by metal bolts and nuts. In Figs. 8 and 9, the BN side limiters are prior to the antenna straps by ~25 mm and do not have the full coverage of the whole antenna module. However, more BN plates can be easily appended if a full coverage is needed. The real shielding effects of BN side limiters, as well as the impurity control, need to be studied and improved through experiments. This will be an indispensable process that has been experienced in other AWCD experiments.

From the description above, we can find that the antenna system is designed to have the minimum requirement for manufacture and installation. These antenna modules can be rapidly made and also can be easily assembled and installed in the vacuum vessel of the SUNIST device. Besides the four insulated bolts to fix the whole antenna structures, the antenna module has no more contacts with the vacuum vessel. The only modification to the vacuum vessel is to weld four nuts on the wall, which are used to mount the antenna module. The direction of the antenna straps, which may be important since the pitch angle of field lines, can be easily modified by changing the position of welded nuts and rotating the CF-200 flange. Of course, this modification cannot be too large since the curvature of the vacuum vessel.

5.2. Mechanical and thermal analysis

Because the parameters of ohmic plasmas in SUNIST are low, e.g., the plasma current is normally 30 kA and the pulse length

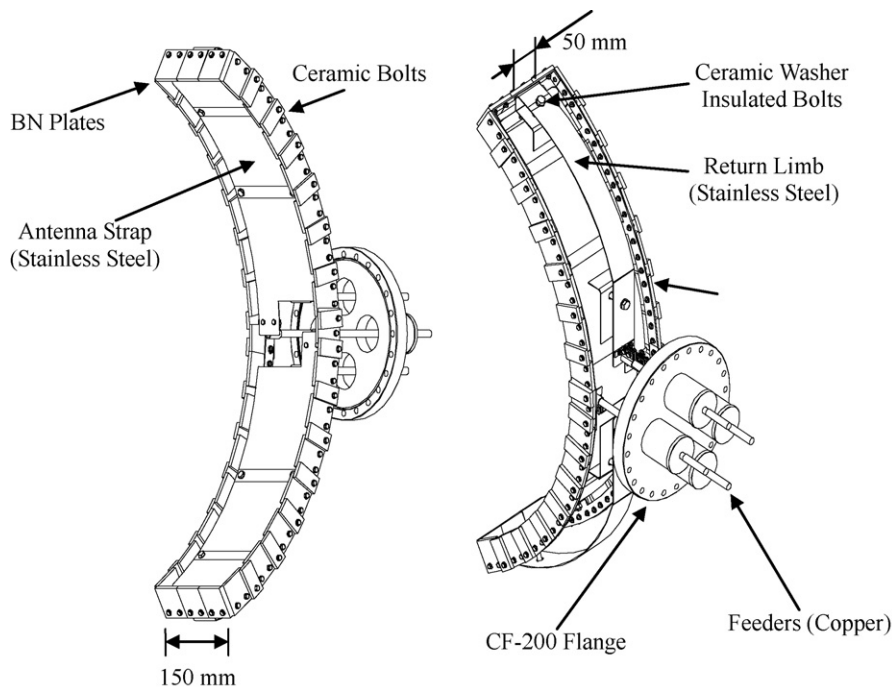


Fig. 9. Three-dimensional view of one antenna module.

is less than 30 ms, the mechanical and thermal risks are not very serious. The removal of Faraday shield makes it is not very critical to analysis the mechanical load during a plasma disruption. The good resilient capability on major disruption of ST plasmas [25] contributes another important effect on simplifying the mechanical and thermal requirements. In SUNIST, typical ohmic discharges have the decay rate of the plasma current is less than 10 MA/s. In the discharges ended with internal reconnection events (IREs), the decay rate is still less than 30 MA/s. Both are very safe values. Therefore, the risk of electromagnetic force applied on the antenna induced by plasma disruption is greatly reduced. In addition, stainless steel straps with a thickness of 1 mm are flexible when shocked by a large momentum. The straps can be bend preventing other parts of the antenna module from damage.

In the magnetic field of SUNIST, i.e., 1500 G, 1 kA dc current in the antenna strap will induce an electromagnetic force of 150 N per meter. This mechanical load will maximally induce a deflection of 9.5 mm on our stainless steel antenna strap with a thickness of 1 mm. The deflections induced by the opposite currents flowing in antenna straps and return limbs are much smaller than this value. However, if we can ensure only RF ac currents can flow in antenna straps these effects will be eliminated.

The thermal problem is not very important in our application. As described in Section 5.1, the ohm loss of the RF current in antenna straps is not significant since the pulse length is limited within 30 ms. In an extreme condition, if the energy of the ohmic power supply (stored in capacitor banks, totally 27.4 kJ) is solely deposited at one antenna strap in a discharge, the temperature rise is merely 100K and is still tolerable.

5.3. The layout of the experimental system

The layout of the experimental system is shown in Fig. 10. Since the operating frequency is as low as 0.4–1 MHz, LC resonant circuits are utilized instead of stub tuner. The antenna units plus short coaxial transmission lines acts as a part of the inductor in LC resonant circuits. The RF generator mainly consists of four triodes excites the

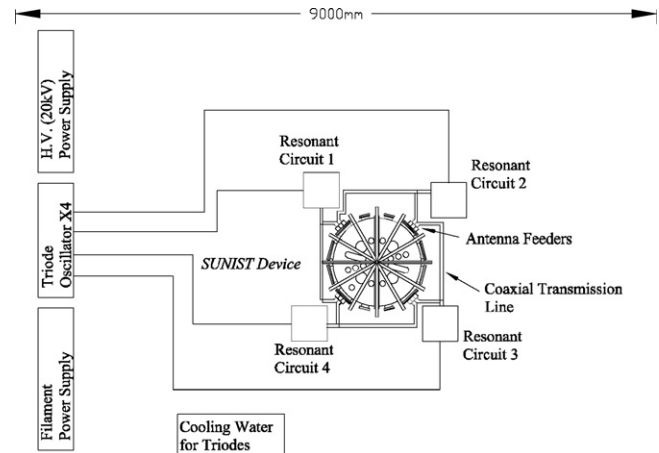


Fig. 10. Layout of the experimental system for Alfvén wave current drive on SUNIST.

oscillation and has the ability of delivering 4×100 kW phased RF power to the antenna straps.

6. Summary and discussion

One dimensional MHD analyses of two concepts of the antenna system provide guidelines for the engineering design and roughly predict the characteristics of power deposition in the future experiments. The folded concept is eventually adopted. The folded antenna system is designed to have best coupling efficiency within the limited space. Side limiters made by BN plates are designed to be simple but effective plasma shielding components. Since the parameters of SUNIST ohmic plasmas are not very high, mechanical and thermal problems are not critical in this antenna system.

This antenna system is rapidly designed using a 1-D MHD model without concerning the important shaping effects of ST plasmas. The experimental measurements of plasma impedances using this antenna system would be the crucial task before injecting high power RF waves. These measurements will give us a clear view of

Alfvén wave spectrum in ST plasmas and a verification of this 1-D MHD model. High power experiments should be conducted based on these impedance measurements.

RF sheath and its effects on impurities would be another important issue that should be experimentally studied. The RF sheath near the ceramic washer insulated bolts is rather critical. The status of the antenna system must be carefully monitored during experiments.

Acknowledgements

The authors appreciate the discussion with Dr. L.F. Ruchko. He also greatly helped the author in checking the results of analyses. The discussions with Dr. R. Majeski and Dr. S. Wukitch are also detailed and very helpful. The author is grateful for the warm-hearted cooperation of Mr. L. Zeng and Mr. L.L. Peng.

This work is supported by NSFC under Grant No. 10535020 and the Foundation for the Author of National Excellent Doctoral Dissertation of PR China under Grant No. 200456.

References

- [1] Y.K.M. Peng, D.J. Strickler, Features of spherical torus plasmas, *Nuclear Fusion* 26 (6) (1986) 769–777.
- [2] A. Sykes, Progress on spherical tokamaks, *Plasma Physics and Controlled Fusion* 36 (1994) B93–B106.
- [3] Y.K.M. Peng, The physics of spherical torus plasmas, *Physics of Plasmas* 7 (2000) 1681.
- [4] A. Sykes, Overview of recent spherical tokamak results, *Plasma Physics and Controlled Fusion* 43 (12A) (2001) 127–139.
- [5] N.J. Fisch, C.F.F. Karney, Current generation with low-frequency waves, *Physics of Fluids* 24 (1) (1981) 27–39.
- [6] S. Wukitch, M. Vukovic, R. Breun, D. Brouchous, D.A. Diebold, M. Doczy, et al., Experimental-evidence of low-frequency current drive in the Phaedrus-T tokamak, *Physical Review Letters* 74 (12) (1995) 2240–2243.
- [7] L.F. Ruchko, E.A. Lerche, R.M.O. Galvao, A.G. Elfimov, I.C. Nascimento, W.P. de Sa, et al., The analysis of Alfvén wave current drive and plasma heating in TCABR tokamak, *Brazilian Journal of Physics* 32 (2002) 57–64.
- [8] R.J. Bickerton, J.W. Connor, J.B. Taylor, Diffusion-driven plasma currents and bootstrap tokamak, *Nature (London) Physical Science* 229 (1971) 110–112.
- [9] T. Ohkawa, Plasma current drive by injection of photons with helicity, *Comments on Plasma Physics and Controlled Fusion* 12 (3) (1989) 165–169.
- [10] Z. Gao, N.J. Fisch, H. Qin, Nonlinear ponderomotive force by low frequency waves and nonresonant current drive, *Physics of Plasmas* 13 (11) (2006), 112307-1-6.
- [11] Z. Gao, N.J. Fisch, H. Qin, J.R. Myra, et al., Nonlinear nonresonant forces by radio-frequency waves in plasmas, *Physics of Plasmas* 14 (8) (2007), 084502-1-4.
- [12] S. Puri, R. Wilhelm, Kinetic-Alfvén-wave current drive in elongated-cross-section plasmas, in: *The 8th topical conference on radio-frequency power in plasmas*, Irvine, USA, 1989, pp. 458–461.
- [13] V.S. Tsypin, I.C. Nascimento, R.M.O. Galvao, Y.K. Kuznetsov, On a bootstrap-like mechanism of radio frequency wave current drive in tokamaks, *Physics of Plasmas* 7 (2000) 1060.
- [14] V.S. Tsypin, R.M.O. Galvao, I.C. Nascimento, M. Tendler, J.H.F. Severo, L.F. Ruchko, Role of trapped and circulating particles in inducing current drive and radial electric field by Alfvén waves in tokamaks, *Journal of Plasma Physics* 67 (05) (2002) 301–308.
- [15] L.F. Ruchko, R.M.O. Galvao, The analysis of Alfvén wave antenna implementation in the ETE spherical tokamak, *Brazilian Journal of Physics* 34 (2004) 1722–1728.
- [16] Y.X. He, A research program of spherical tokamak in China, *Plasma Science and Technology* 4 (4) (2002) 1355–1360.
- [17] S. Cuperman, C. Bruma, K. Komoshvili, Aspect-ratio dependence of Alfvén-wave current drive and its efficiency in simulated tokamak plasmas. A systematic, full-wave equation investigation, *Journal of Plasma Physics* 59 (1998) 461–498.
- [18] S. Cuperman, C. Bruma, K. Komoshvili, The combined toroidicity, ellipticity and triangularity effects on the energy deposition of Alfvén modes in pre-heated, low aspect ratio tokamaks, *Physics Letters A* 362 (4) (2007) 305–323.
- [19] S. Cuperman, C. Bruma, K. Komoshvili, Solution of the resistive two-fluid wave equations for Alfvén modes in spherical tokamak plasmas, *Journal of Plasma Physics* 69 (01) (2003) 15–43.
- [20] R. Behn, A.d. Chambrier, G.A. Collins, P.-A. Duperrex, A. Heym, F. Hofmann, et al., Recent Alfvén wave heating results on the TCA tokamak, *Plasma Physics and Controlled Fusion* 26 (1A) (1984) 173–182.
- [21] K. Appert, J. Vaclavik, Effects of finite ion cyclotron frequency on the absorption of magnetohydrodynamic waves at the spatial Alfvén resonance, *Plasma Physics* 25 (5) (1983) 551–561.
- [22] L.F. Ruchko, M.C.R. Andrade, R.M.O. Galvao, Influence of conducting side limiters on the excitation of Alfvén waves in tokamak plasmas, *Nuclear Fusion* 36 (4) (1996) 503–508.
- [23] K. Appert, J. Vaclavik, L. Villard, Spectrum of low-frequency, nonaxisymmetric oscillations in a cold, current-carrying plasma column, *Physics of Fluids* 27 (1984) 432.
- [24] J. Sorensen, D.A. Diebold, R. Majeski, N. Hershkowitz, Edge power deposition reduction in a tokamak by replacing the Faraday screen, *Nuclear Fusion* 36 (2) (1996) 173.
- [25] A. Sykes and the START, NBI, MAST and Theory Teams, The spherical tokamak programme at Culham, *Nuclear Fusion* 39 (9y) (1999) 1271–1281.